Hue University Journal of Science: Natural Science
Vol. 131, No. 1D, 13–21, 2022

pISSN 1859-1388
eISSN 2615-9678

Nonlinear properties of circular solid-core photonic crystal fiber with air-hole diameter difference and spacing in the cladding

Tran Tran Bao Le[1], Trong Dang Van[1], Lanh Chu Van[1], Trang Nguyen Thi Ha[1], Duc Hoang Trong[2], Thuy Nguyen Thi[2]*

[1] Department of Physics, Vinh University, 182 Le Duan St., Vinh City, Viet Nam
[2] University of Education, Hue University, 34 Le Loi St., Hue, Viet Nam

* Correspondence to Thuy Nguyen Thi <ntthuy@hueuni.edu.vn>

(*Received: 30 January 2022; Accepted: 24 February 2022*)

Abstract. We emphasize the ability to control the nonlinear properties of silica-based circular solid-core photonic crystal fibers (PCFs) with a new design. In this fiber, the diameter of the air hole in the rings is different, and the lattice constant is ununiform in the cladding. The simulation results show that a near-zero ultra-flattened chromatic dispersion over a wide wavelength range and low attenuation in these PCFs is achieved. Two structures with the lattice constant, Λ, of 0.7 and 0.9 μm and filling factor, d_1/Λ, of 0.45 in the first ring were selected and investigated in detail. These structures are capable of generating broad-spectrum supercontinuum.

Keywords: photonic crystal fiber, circular lattice, supercontinuum generation, near-zero ultra-flattened chromatic dispersion, low attenuation

1 Introduction

Photonic crystal fibers (PCFs) are a class of optical fiber based on the properties of photonic crystals. It was first announced in 1996 at the Optic fiber conference by Russell and his colleagues [1]. Since then, PCFs have attracted the attention of scientists because of the fiber special and unique properties in design and construction that are not present in conventional optical fibers. They can be designed flexibly by changing structural parameters, such as lattice shape (circle, square or hexagonal), shape and size of air holes, and solid or hollow core. This allows PCFs not only to have applications like conventional optical fibers but also to have special applications in various fields, such as lasers, amplifiers, dispersion compensators, nonlinear processing, optical devices [2], electrically tunable [3, 4], ultra-flattened dispersion [5, 6], optofluidic devices [7], dispersion compensation [8], and high-sensitivity sensing and supercontinuum generation [9-17].

The most commonly used types of lattice are circular, square, and hexagonal lattices published in the last few years, including new designs of the large mode area circular lattice [18], the circular lattice with high negative dispersion [19], the low confinement loss in hexagonal lattice [20], the square lattice with an ultra-broadband and compact [21], and the most recently published studies [22] for all three types of lattices. All these publications only focused on studying the characteristic quantities of fibers but did not apply to supercontinuum generation. Besides, the difference in air-hole diameters of the lattice rings and the distance between air holes in the cladding have not been emphasized in those publications.

In this paper, we present circular lattice solid-core PCFs that have a difference in the stomatal diameters of the first ring near the core compared with other rings in the cladding. In addition, the heterogeneity in the distance between two air holes in the structure is also emphasized. Specifically, the centre of the air holes in the first ring is 1.095 times the lattice constant (Λ) from the centre of the circular lattice, while the distance between the centre of the second-ring air holes and that of the lattice ring is kept constant at twice of the lattice constant (2 × Λ). The air holes in the remaining rings are equally spaced with Λ. With these differences, the structures are designed to improve the optical properties of the PCFs. We investigated the effect of key structural parameters, including filling factor, d_1/Λ, and lattice constant, Λ, on the nonlinear characteristics of PCFs. Hence, we proposed two optimal fibers (Λ = 0.7 μm; d_1/Λ = 0.45 and Λ = 0.9 μm; d_1/Λ = 0.45) for super-continuum generation.

2 Numerical modeling

The solid-core PCFs used in the numerical analysis of this paper are in the form of a circular lattice. The circular PCF structure was chosen for investigation because it has outstanding advantages compared with other lattices. With its high symmetry, this lattice restricts the light entering the core and increases its nonlinearity, providing a higher super-continuum generation efficiency and, thus, a higher bandwidth than other lattices. The base material is fused silica that creates a large difference in the refractive index of the core and the mantle to enhance light restriction in the core. Fig. 1 shows the geometry of the PCF in our design. The fiber consists of eight air-hole rings arranged in an orderly manner in the shell. These structures were designed with the Lumerical Mode Solution software [23].

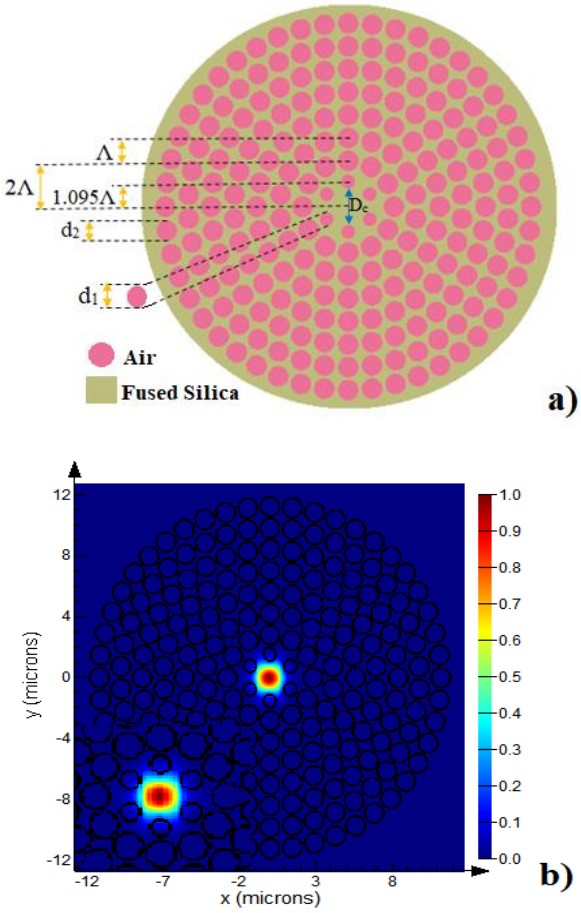

Fig. 1. Geometrical structure diagram (a) and intensity distribution (b) in the silica-based PCF with circular lattice

Saitor et al. [24] proved that the characteristic quantities of PCFs are strongly influenced by the difference in the size of air holes in the lattice rings. The hole size in the first ring has a direct effect on dispersion, including the flatness and normal or anomalous properties of dispersion, even the shift of the zero dispersion wavelength (ZDW). In contrast, the mode attenuation is dominated by the remaining loops. Hence, we designed a PCF structure with air holes in the first ring (near the core) with a diameter, d_1, corresponding to the filling factor, d_1/Λ, where d_1/Λ changes from 0.3 to 0.75 with an increment of 0.05. The air-hole diameters, d_2, of the remaining lattice rings is constant (0.9 × Λ). Furthermore, in

pISSN 1859-1388
eISSN 2615-9678

previous studies, the PCF has a distance between the centre of the air holes equal to Λ; however, there is a difference in these parameters in our design. Specifically, while the centre of the circular lattice is 1.095 × Λ from the centre of the first ring air holes, the spacing to the centre of the air holes in the second ring remains the same at 2 × Λ. The air holes in the remaining rings are at an equal distance apart. The core diameter, depending on d_1 and Λ, is determined according to the formula $D_c = 2 \times 1.095 \times \Lambda - d_1$. In the simulation, we use the lattice constant of 0.7, 0.9, and 1.4 μm. The structural parameters of the PCFs are presented in Table 1. New features of our design result in minimal attenuation, controlling chromatic dispersion for optimal dispersion.

Table 1. Parameters of PCFs structures for simulations

Λ = 0.7 μm										
d_1/Λ	0.3	0.35	0.4	0.45	0.5	0.55	0.6	0.65	0.7	0.75
d_1	0.21	0.245	0.28	0.315	0.35	0.385	0.42	0.455	0.49	0.525
D_c	1.323	1.288	1.253	1.218	1.183	1.148	1.113	1.078	1.043	1.008
Λ = 0.9 μm										
d_1/Λ	0.3	0.35	0.4	0.45	0.5	0.55	0.6	0.65	0.7	0.75
d_1	0.27	0.315	0.36	0.405	0.45	0.495	0.54	0.585	0.63	0.675
D_c	1.701	1.656	1.611	1.566	1.521	1.476	1.431	1.386	1.341	1.296
Λ = 1.4 μm										
d_1/Λ	0.3	0.35	0.4	0.45	0.5	0.55	0.6	0.65	0.7	0.75
d_1	0.42	0.49	0.56	0.63	0.7	0.77	0.84	0.91	0.98	1.05
D_c	2.646	2.576	2.506	2.436	2.366	2.296	2.226	2.156	2.086	2.016

3 Simulation results and analysis

The refractive index of fused silica as a function of the wavelength is described with the Sellmeier formula (Eq. 1) [25].

$$n^2_{\text{Fused silica}}(\lambda) = 1 + \frac{0.6694226\lambda^2}{\lambda^2 - 4.4801\times10^{-3}} + \frac{0.4345839\lambda^2}{\lambda^2 - 1.3285\times10^{-2}} + \frac{0.8716947\lambda^2}{\lambda^2 - 95.341482} \quad (1)$$

Fig. 2 presents the effective refractive index (n_{eff}) of the fundamental modes calculated for the structures with the first ring filling factor varying from 0.3 to 0.75 and the lattice constants of 0.7, 0.9, and 1.4 μm. In our cases, the effective refractive index of the PCFs changes with the wavelength, lattice constant, and filling factor and has a similar shape. It can be seen that as the wavelength increases, the effective refractive index decreases significantly. The reason is that light penetration into PCF cladding at longer wavelengths is stronger than at shorter ones [26]. An increase in d_1/Λ of the PCFs at a particular wavelength reduces the effective refractive index, but it increases with an increase in Λ. It can be observed that the change in effective refractive index is

mainly influenced by d_1/Λ and Λ. To see this difference clearly, we determined the real value of the effective refractive index of the fibers with different values of Λ and d_1/Λ at a wavelength of 1.55 μm, presented in Table 2. The effective refractive index of PCF has the largest value, with a filling factor of 0.3 and the smallest, with d_1/Λ being 0.75 in the same lattice constant.

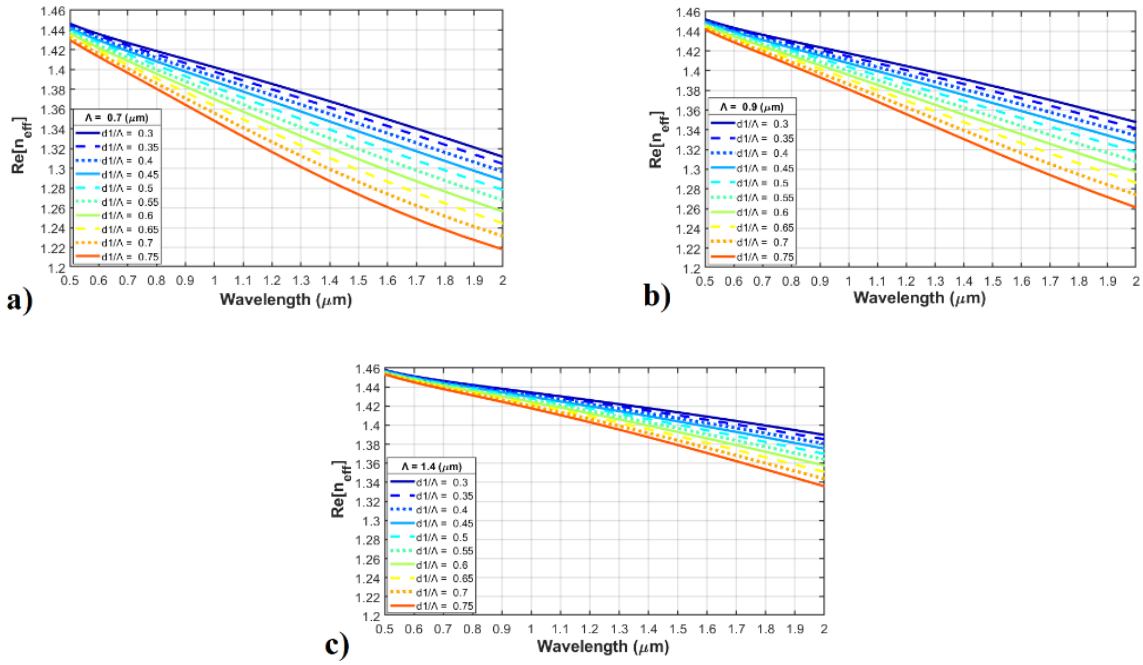

Fig. 2. Real part of effective refractive index as function of wavelength of PCFs with various d_1/Λ when (a) Λ = 0.7 μm, (b) Λ = 0.9 μm, and (c) Λ = 1.4 μm

Table 2. Real part of the effective refractive index of silica-based PCFs at 1.55 μm wavelength with various lattice constants and linear filling factors of the first ring

λ (μm)	d_1/Λ	$Re[n_{eff}]$		
		Λ = 0.7 μm	**Λ = 0.9 μm**	**Λ = 1.4 μm**
1.55	0.3	1.354	1.381	1.411
	0.35	1.348	1.376	1.408
	0.4	1.34	1.37	1.405
	0.45	1.332	1.363	1.401
	0.5	1.324	1.356	1.398
	0.55	1.314	1.349	1.394
	0.6	1.304	1.34	1.389
	0.65	1.292	1.332	1.385
	0.7	1.28	1.322	1.38
	0.75	1.267	1.312	1.375

pISSN 1859-1388
eISSN 2615-9678

Dispersion is an important factor of PCFs in supercontinuum generation. The ZDW values and the flatness of dispersion are governed by the structure and composition of PCF. The total dispersion (D) as a function of wavelength depends on the effective refractive index of the propagation mode and is determined according to the following formula [27].

$$D = -\frac{\lambda}{c}\frac{d^2\,\mathrm{Re}\left[n_{\mathrm{eff}}\right]}{d\lambda^2} \qquad (2)$$

where Re[n_{eff}] is the real part of the effective refractive index and c is the speed of light in the vacuum.

The dependence of dispersion on wavelength and variation of the filling factor and the lattice constant of PCFs are shown in Fig. 3. From these data, we can see that the dispersion of PCFs is strongly influenced by the change in the filling factor and the lattice constant. The obtained dispersion is quite diverse, with normal and anomalous dispersion with one ZWD and two ZWDs achieved in the studied wavelength region. This is one of the advantages of our study compared with previous works [19, 28] that only achieve anomalous dispersion. In addition, the change in these structural parameters leads to a shift in ZWD to longer wavelengths. At the lattice constant of 0.7 μm (PCFs with the smallest core diameter of the three studied lattice constants), the dispersion is quite diverse, with normal and anomalous dispersion with one ZWD and two ZWDs (Fig. 3a). The normal dispersion curves were obtained for the filling factor of 0.45–0.65 and anomalous dispersion curves with one ZWD begin to appear with d_1/Λ being 0.3. In contrast, the dispersion curves of the remaining fibers intersect the zero-dispersion line at two points, i.e. anomalous dispersion with two ZWDs in this case. In particular, the PCF with d_1/Λ being 0.45 at the lattice constant of 0.7 μm exhibits all-normal dispersion, and its curve is asymptotic to the zero-dispersion in the wavelength range of 1.1–1.4 μm, which gives a high efficiency of super-continuum generation in the near-infrared region.

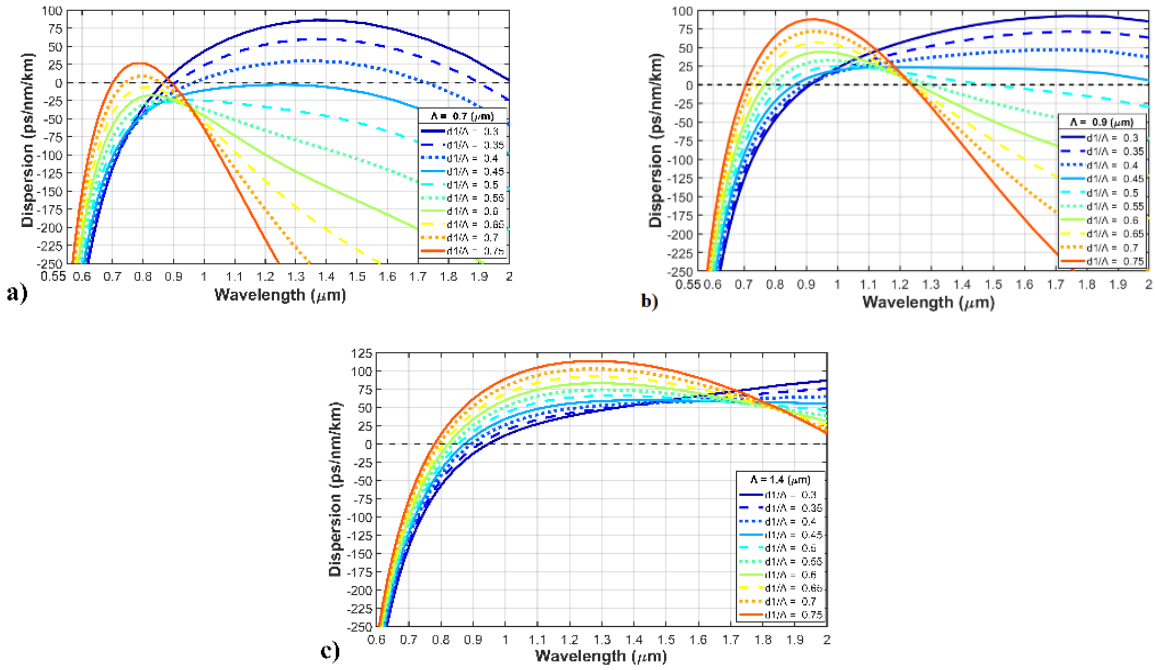

Fig. 3. Dispersion as function of wavelength of PCFs with various d_1/Λ for (a) Λ = 0.7 μm, (b) Λ = 0.9 μm, and (c) Λ = 1.4 μm

Varying the lattice-constant values results in a change in the core diameter, D_c, which causes the dispersion profile to change, including the shift of the ZWD. At a large lattice constant (0.9 μm, Fig. 3b), all-normal dispersion curves are no longer present; instead, there are anomalous dispersion curves with one ZWD and two ZWDs. The dispersion at the filling factor of 0.45 is very flat over a wide wavelength range from 1.1 to 1.6 μm despite the transition from all-normal dispersion to anomalous dispersion. Furthermore, only anomalous dispersion curves with one ZWD are obtained when Λ = 1.4 μm (larger core). It can be seen that the dispersion characteristics in our design can be controlled with the variation of the filling factor, d_1/Λ, and the lattice constant, Λ.

From the simulation results, we propose two PCFs with excellent dispersion, #F_1 and #F_2, to analyze for supercontinuum generation. Their structural parameters are presented in Table 3.

Fig. 4 presents the dispersion characteristics of the proposed PCFs. The #F_1 fiber with the all-normal ultra-flat dispersion curve is very close to the zero-dispersion line and can produce a wide SC spectrum. In contrast, the #F_2 fiber has a flat anomalous dispersion curve with one ZWD at 0.863 μm. The pump wavelengths chosen for fibers #F_1 and #F_2 are 1.24 and 0.86 μm. The characteristics of the proposed PCFs are compared with those of previous publications (Table 4). The dispersion values at the pump wavelength of the #F_1 and #F_2 fibers are –2.944 and –0.8 ps·nm·km^{-1}.

The effective mode area of the proposed PCFs is shown in Fig. 5. It can be seen that the effective mode area of the two fibers increases linearly with increasing wavelength. Because of its larger core diameter, #F_2 always has a larger effective mode area than #F_1. At the pump wavelength, fibers #F_1 and #F_2 have an effective mode area of 1.879 and 1.908 μm^2.

The nonlinear coefficient is inversely proportional to the effective mode area according to the formula $\gamma = 2 \times \pi \times n_2/\lambda \times A_{eff}$ [29], so it tends to decrease linearly with an increase in wavelength (Fig. 6). Fiber #F_1 always has greater nonlinearity than #F_2, and at the pump wavelength, the former has a nonlinear value of 90.415 W^{-1}·km^{-1}, while that of the latter is 63.654 W^{-1}·km^{-1}.

The attenuation of fundamental mode according to the wavelength is shown in Fig. 7. In the proposed fibers, the attenuation value of #F_2 almost coincides with the horizontal axis in the entire investigated wavelength range. While the attenuation of the two fibers is similar at wavelengths less than 1.7 μm, we observe a significant increase in the attenuation of #F_1 when the wavelength increases from 1.7 to 2 μm. At the pump wavelength, the attenuation values of #F_1 and #F_2 are 1.884E–09 and –9.931E–20 dB·m^{-1}. A very small attenuation is the advantage of our model. Therefore, it can be seen that the characteristic quantities of the analyzed fibers are suitable for super-continuum generation.

Table 3. Structural parameters of proposed PCFs

#	**Λ (μm)**	d_1/Λ	D_c **(μm)**
#F_1	0.7	0.45	1.218
#F_2	0.9	0.45	1.566

pISSN 1859-1388
eISSN 2615-9678

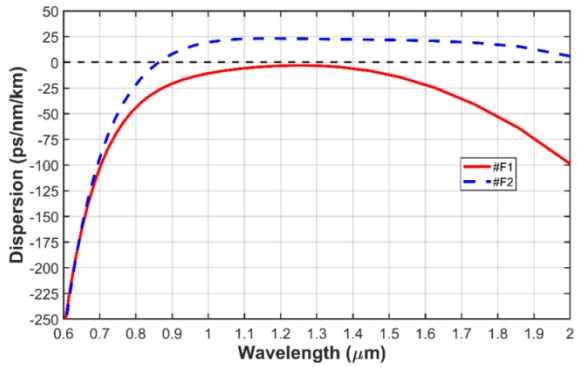

Fig. 4. The dispersion properties of the proposed PCFs

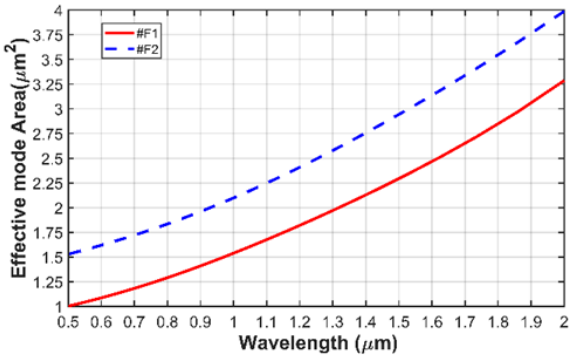

Fig. 5. The effective mode area properties of the proposed PCFs

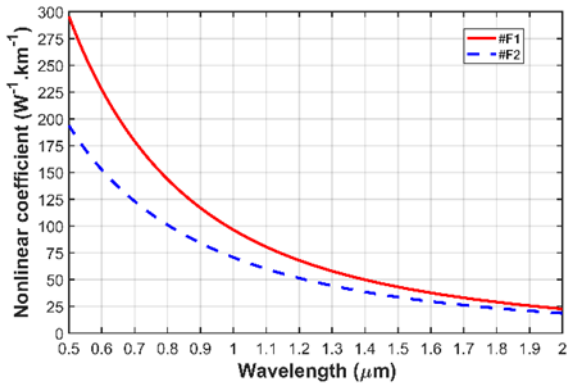

Fig. 6. The nonlinear coefficients of the proposed PCFs

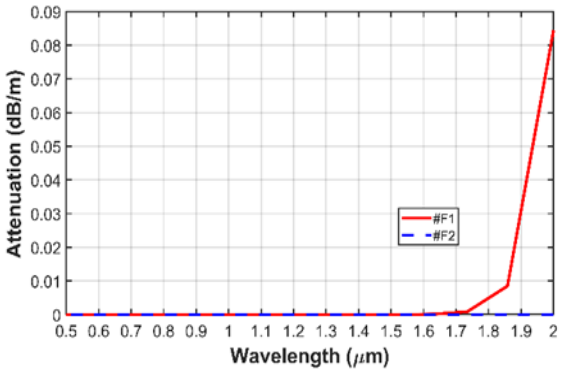

Fig. 7. The attenuation properties of the proposed PCFs

Table 4. Characteristic values of proposed PCFs in comparison with previous publications

Photonic crystal fibers	Year	D_c (μm)	Pump wavelength (μm)	D (ps·nm^{-1}·km^{-1})	Attenuation (dB/m)	A_{eff} (μm^2)	γ (W^{-1}·km^{-1})
[30]	2011	–	1.8	<50	<0.038	1810	–
[14]	2017	3.34	1.55	–9.46	192	7.8	1200
[7]	2020	2.34	1.56	–2.2	240	4.73	2000
#F_1	this work	1.218	1.24	–2.944	1.884E–09	1.879	63.654
#F_2	this work	1.566	0.86	–0.8	–9.931E–20	1.908	90.415

4 Conclusion

In this paper, we designed circular lattice photonic crystal fibers with the difference in the first-ring air-hole diameter and the distance of the air holes in the cladding. With this difference, the characteristic properties of PCFs can be controlled via the variation of the filling factor, d_1/Λ, and the lattice constant, Λ. The photonic crystal fibers give diverse dispersion results, including ultra-flattened near-zero all-normal dispersion curves

in a wide wavelength range as well as an anomalous dispersion regime with one and two ZWDs. Two structures were proposed for detailed analysis. They have optimal dispersion, high nonlinearity and low attenuation, which are the strong points of our design. These advantages are essential factors for super-continuum generation.

Funding statement

This research was funded by Vingroup JSC and supported by the Master and PhD's Scholarship Programme of Vingroup Innovation Foundation (VINIF), Institute of Big Data, under code VINIF.2021.TS.155.

References

1. Knight JC, Birks TA, Russell PSJ, Atkin DM. All-silica single-mode optical fiber with photonic crystal cladding. Optics Letters. 1996;21(19):1547-2.
2. Larsen T, Bjarklev A, Hermann D, Broeng J. Optical devices based on liquid crystal photonic bandgap fibers. Optics Express. 2003;11(20):2589.
3. Yu C, Liou J. Selectively liquid-filled photonic crystal fibers for optical devices. Optics Express. 2009;17(11):8729.
4. Du F, Lu YQ, Wu ST. Electrically tunable liquid-crystal photonic crystal fiber. Applied Physics Letters. 2004;85(12):2181.
5. Noordegraaf D, Scolari L, Lægsgaard J, Rindorf L, Alkeskjold TT. Electrically and mechanically induced long period gratings in liquid crystal photonic bandgap fibers. Optics Express. 2007; 15(13):7901.
6. Gundu KM, Kolesik M, Moloney JV, Lee KS. Ultra-flattened-dispersion selectively liquid-filled photonic crystal fibers. Optics Express. 2006; 14(15): 6870.
7. Rasmussen PD, Lægsgaard J, Bang O. Chromatic dispersion of liquid-crystal infiltrated capillary tubes and photonic crystal fibers. Journal of the Optical society of America B. 2006;23(10):2241.
8. Park J, Kang D, Paulson B, Nazari T, Oh K. Liquid core photonic crystal fiber with low-refractive-index liquids for optofluidic applications. Optic Express. 2014;22(14):17320.
9. Lanh CV, Thuy HV, Long CV, Borzycki K, Khoa DX, Vu TQ, et al. Supercontinuum generation in photonic crystal fibers infiltrated with nitrobenzene. Laser Physics. 2020;30(3):035105.
10. Lanh CV, Thuy HV, Long CV, Borzycki K, Khoa DX, Vu TQ, et al. Optimization of optical properties of photonic crystal fibers infiltrated with chloroform for supercontinuum generation. Laser Physics. 2019;29(7): 075107.
11. Khoa DX, Lanh CV, Quang HD, Luu VX, Trippenbach M, Buczynski R. Dispersion characteristics of a suspended-core optical fiber infiltrated with water. Applied Optics. 2017;56(4): 1012-1019.
12. Khoa DX, Lanh CV, Long CV, Quang HD, Luu VM, Trippenbach M, et al. Influence of temperature on dispersion properties of photonic crystal fibers infiltrated with water. Optical and Quantum Electronics. 2017;49(2).
13. Quy HQ, Lanh CV. Spectrum Broadening of Supercontinuum Generation by fill Styrene in core of Photonic Crystal Fibers. Indian Journal of Pure & Applied Physics. 2021;59:522-527.
14. Lanh CV, Anuszkiewicz A, Ramaniuk A, Kasztelanic R, Khoa DX, Trippenbach M, et al. Supercontinuum generation in photonic crystal fibers with core filled with toluene. Journal of Optics. 2017;19(12):125604.
15. Vu NQ, Linh DT, Vu TQ, Khoa DX, Ha LTK, Thu ND, et al. Comparison of characteristics quantities of photonic crystal fiber with hollow core infiltrated Nitrobenzene and Toluene at 1064nm for supercontinuum generation. Journal of Military Science and Technology. 2019; 61:183-188.
16. Lanh CV, Vu NQ, Linh NTM, Vu TQ, Trang CTG, Huyen DT, et al. Dispersions of solid-core Silica PCFs infiltrated with Water and Ethanol fo supercontinuum generation. In: Hung ND, editor. Advances in Applied and Engineering Physics. Proceedings of CAEP(VI); 2019 October 22-26; Thai Nguyen; Hanoi: Publishing House for Science and Technology; 2020. p. 288-291.
17. Linh DT, Huyen PN, Vu NQ, Huong NL, Vu TQ, Khoa DX, et al. Optimization of characteristic parameters of photonic crystal fiber with core infiltrated by Carbon disulfide liquid for

pISSN 1859-1388
eISSN 2615-9678

supercontinuum generation. In: Hung ND, editor. Advances in Applied and Engineering Physics. Proceedings of CAEP(V); 2017 October 2-4; Da Lat; Hanoi: Publishing House for Science and Technology; 2018. p. 206-211.

18. Medjouri A, Simohamed AM, Ziane O, Boudrioua A. Analysis of a new circular photonic crystal fiber with large mode area. Optik- International Journal for Light and Electron Optics.2015;126(24):5718-5724.

19. Pandey SK, Prajapati YK, Maur JB. Design of simple circular photonic crystal fiber having high negative dispersion and ultra-low confinement loss. Results in Optics. 2020;1:100024.

20. Sen S, Abdullah-Al-Shafi Md, Kabir MA. Hexagonal photonic crystal Fiber (H-PCF) based optical sensor with high relative sensitivity and low confinement loss for terahertz (THz) regime. Sensing and Bio-Sensing Research. 2020;30:100377

21. Wang Y, Li S, Wu J, Yu P, Li Z. Design of an ultrabroadband and compact filter based on square-lattice photonic crystal fiber with two large gold-coated air holes. Photonics and Nanostructures - Fundamentals and Applications. 2020;41:100816.

22. Tran LTB, Thuy NT, Ngoc VTM, Trung LC, Minh LV, Long VC, et al. Analysis of dispersion characteristics of solid-core PCFs with different types of lattice in the claddings, infiltrated with ethanol. Photonics Letters of Poland. 2020;12(4): 106-108.

23. ANSYS Inc. Lumerical Mode Solution software. Version 2021. United States: ANSYS; https://doi.org/https://www.lumerical.com/products/mode

24. Saitoh K, Koshiba M, Hasegawa T, Sasaoka E. Chromatic dispersion control in photonic crystal fibers: application to ultra-flattened dispersion. Optics Express. 2003;11:843-852K.

25. Moutzouris K, Papamichael M, Betsis SC, Stavrakas I, Hloupis G, Triantis D. Refractive, dispersive and thermo-optic properties of twelve organic solvents in the visible and near-infrared. Applied Physics B. 2014;116(3):617.

26. Dhara P, & Singh V K. Investigation of rectangular solid-core photonic crystal fiber as temperature sensor. Microsystem Technologies. 2021;27:127-132

27. Buczyński R. Photonic crystal fibers. Acta Physica Polonica A. 2004;106(2):141-168.

28. Pniewski J, Stefaniuk T, Hieu LV, Long VC, Lanh CV, Kasztelanic R, et al. Dispersion engineering in nonlinear soft glass photonic crystal fibers infiltrated with liquids. Applied Optics. 2016; 55(19):5033-5040.

29. Knight JC, Birks TA, Cregan RF, Russell PSJ. Large Mode area photonic crystal fiber. Optics Photonics News. 1998;9(12):34-35.

30. Napierala M, Nasilowski T, Pawlik EB, Mergo P, Berghmans F, Thienpont H. Larger-mode-area photonic crystal fiber with double lattice constant structure and low bending loss. Optics Express. 2011;19(23):22628.